Full text open access online (Since 2001)

PRINT: ISSN 0972-3757 ONLINE: ISSN 2456-6330
Int J Hum Genet, 24(3): 306-317 (2024)
DOI: 10.31901/24566322.2024/24.03.835

MiR-148a Down-regulates HPIP Expression to Mediate Immune Escape of Non-small Cell Lung Cancer A549 Cells

Jilian Ren[1*], Xiaoxia Hao[1] and Xiaoyan Li[2]

[1]Fenyang College of Shanxi Medical University, Fenyang 032200, Shanxi Province, China
[2]Fengyang Affiliated Hospital of Shanxi Medical University, Fenyang 032200, Shanxi Province, China

KEYWORDS HPIP. miR-148a. NK Cells. NSCLC. OS

ABSTRACT The researchers aimed to explore the role of miR-148a in mediating the immune escape of non-small cell lung cancer (NSCLC) A549 cells through its regulatory effects on hematopoietic pre-B-cell leukaemia transcription factor-interacting protein (HPIP) expression. For NSCLC patients, there was a relationship between their poor overall survival and high HPIP expression. When HPIP expression was regulated, compared with blank group, si-HPIP group had lower HPIP and sHPIP expression levels and proliferation ability. The lysis rate was higher in NK+anti-ILT-2 group than in NK group while higher in NK+Scramble+anti-ILT-2 group than in NK+Scramble group at the effector-to-target ratios of 10 and 5. NK+si-HPIP group exhibited an elevated lysis rate by contrast to NK group at the ratio of 10. The subcutaneous tumour in mice inoculated with A549 cells grew faster than in mice inoculated with si-HPIP-transfected cells. The miR-148a/HPIP axis mediates immune escape and influences cell proliferation to exert its carcinogenic effect on NSCLC.

INTRODUCTION

Alternatively called pre-B-cell leukaemia homeobox-interacting protein 1 (PBXIP1), hematopoietic pre-B-cell leukaemia transcription factor-interacting protein (HPIP) functions as a co-repressor of pre-B-cell leukaemia homeobox 1 to modulate hematopoietic stem cell growth and differentiation while inhibiting the progression of leukaemia (Zhao et al. 2020). HPIP can facilitate the escape of cancer cells from immune surveillance by interacting with immunoglobulin receptors (Jiang et al. 2020b; Pan et al. 2021). It has been confirmed through large quantities of investigations that the primary lesions or serum specimens of patients suffering from non-small cell lung cancer (NSCLC) have an abnormal HPIP expression, suggesting that HPIP and soluble HPIP (sHPIP) are valuable for predicting the prognosis of NSCLC (Duan and Liu 2020; Zhu et al. 2020; Phillips-Chavez et al. 2020). sHPIP in NSCLC patients exists as a prognostic factor independently affecting the overall survival (OS) (Roeper et al. 2020), and reducing the sHPIP level in serum is associated with prolonged OS. In addition, the patients with advanced NSCLC have an elevated serum sHPIP level (Wang et al. 2020).

Several micro ribonucleic acids (miRNAs), such as miR-148a, have regulatory effects on HPIP (He et al. 2021). For instance, a new contraceptive method has been designed based on the mechanism by which miR-148a is delivered into the uterus to offset HPIP expression (Jiang et al. 2020; Li et al. 2021). Besides, the tolerance of HBV infection to antitumor immune response is increased by down-regulating miR-148a, so the HPIP level is up-regulated. Besides, the serum miR-148a level is correlated with NSCLC prognosis (Elnaggar et al. 2021). At present, however, the regulatory mechanism of HPIP for NSCLC remains elusive. Therefore, the correlation between HPIP expression and NSCLC prognosis was investigated herein. Moreover, the effects of HPIP regulated by miR-148a on the invasion, propagation as well as tolerance to natural killer (NK) cell-mediated cytolysis of NSCLC cells were further explored.

Address for correspondence:
Jilian Ren
E-mail: renjlfcsmu@sdsch.cn

Objectives

The present study intended to corroborate that miR-148a/HPIP axis served as a carcinogen to mediate immune escape and impact cell proliferation in the case of NSCLC.

METHODOLOGY

Cells

The Cell Bank/Stem Cell Bank, Chinese Academy of Sciences (Shanghai, China) supplied NK-

92MI cells as well as NSCLC cell lines including H460 (human large cell lung cancer cell), A549 (human lung adenocarcinoma cell) and L78 (human lung squamous cell carcinoma cell). Specifically, EK-Bioscience (Shanghai, China) was the manufacturer of A549, H460 and NK-92MI cells, while L78 cells sourced from Shanghai Yaji Biotechnology Co. Ltd. (China). They were frozen in liquid nitrogen prior to application.

Reagents

Alpha minimal essential medium (α-MEM, Cat. No. 12561056), foetal bovine serum (Cat. No. 16140063), horse serum (Cat. No. 26050088), Lipofectamine™ 2000 Transfection Reagent (Cat. No. 11668500), TRIzol Reagent (Cat. No. 15596018), Roswell Park Memorial Institute (RPMI)-1640 medium (Catalog No. 11875119), mirVana™ miRNA Isolation Kit (Cat. No. AM1561), SYBR Green Polymerase Chain Reaction (PCR) Premix (Cat. No. 4309155) and enhanced chemiluminescence (ECL) solution (Cat. No. 34580) were purchased from Thermo Fisher (USA). 2-Mercaptoethanol (Cat. No. M3148), folic acid (Cat. No. F8758), interleukin (IL)-2 (Cat. No. I2644), formalin (Cat. No. 252549) and crystal violet (Cat. No. C0775) were provided by Sigma (USA). ReverTra Dash Kit (Cat. No. PCR-401) was bought from Toyobo Biotech (Japan). Beijing Solarbio Science and Technology Co. Ltd. provided Methyl thiazolyl tetrazolium (MTT) assay kit (Cat. No. M1020). Beyotime Biotechnology (Shanghai) offered the bicinchoninic acid (BCA) protein assay kit (Cat. No. P0012) plus Dual-luciferase Reporter Gene Assay Kit (Cat. No. RG027). Rabbit HPIP primary antibody (Cat. No. ab176591), immunoglobulin-like transcript (ILT)-2 antibody (Cat. No. ab238145), mouse GAPDH antibody, rabbit secondary antibody and mouse secondary antibody were bought from Abcam (USA). Other commercially available reagents were all of analytical grade.

Apparatus

DNP-9272 electrothermal constant-temperature incubator [Ganyi Instrument and Equipment (Shanghai) Co. Ltd., China], optical microscope (Leica, Germany), ABI-7300 fluorescence quantitative PCR system (Thermo Fisher, USA), Benchtop Multi-Mode Microplate Reader (FlexStation® 3, Molecular Devices, USA), M1324R high speed freezing microcentrifuge (Shenzhen RWD Life Science Co. Ltd., China), LF-Mini4 small vertical electrophoresis tank (Beijing Longfang Technology Co. Ltd., China), eBlot™ L1 Fast Wet transfer System [GenScript (Nanjing) Co. Ltd., China], TS-2000 Decolouring Shaker (Jiangsu Haimen Kylin-Bell Lab Instruments Co. Ltd., China), and Non-destructive Quantitative Touch Imager [e-BLOT Life Science (Shanghai) Co. Ltd. China] were used.

Kaplan-Meier Survival Analysis of NSCLC Patients

KMPlot (www.kmplot.com), a public available microarray database integrating patient data, was employed to analyse the influence of HPIP on NSCLC prognosis. The Kaplan-Meier method was adopted to draw the survival curve, with the optimal cut-off value and appropriate probe automatically selected. The two-tailed time series test from the KMPlot database was utilised to analyse statistical significance. 207838 was the Affymetrix ID number of HPIP.

Cell Culture

RPMI-1640 medium mixed with ten percent foetal bovine serum (Kalani et al. 2021) was employed to incubate A549, L78 and H460 cells. NK-92MI cells were incubated in seventy-five percent α-MEM containing 0.1 mM 2-mercaptoethanol, 200 U/mL recombinant IL-2, 12.5 percent foetal bovine serum, 12.5 percent horse serum, and 0.02 mM folic acid (Anft et al. 2020). The cell incubation was conducted using an incubator under five percent CO_2 at 37°C.

Cell Transfection

A549 cells underwent plate (6 wells) inoculation. Upon reaching eighty percent confluence, the cells were transfected with miR-148a-mimic (5'-AAAGUUCUGAGACACUCCGACU-3'), miR-NC (5'-UCAGCACUUUUUGACAGAACGU-3'), and miR-148a-inhibitor (5'-UCAGUGCACUACAGAACUUUGU-3') using Lipofectamine™ 2000 transfection reagent. The small interfering RNA (siRNA) sequence of HPIP was 5'-TTCTAGGGAGTGGAGTGGA-3', and the sequence of knocked down HPIP was 5'-TCCACTCCACTCCCTAGAA-3'. Negative controls of 5'-ACGUGA-

CACGUUCGGAGAATT-3' plus 5'-UUCUCCGAACGUGUCACGUTT-3' were utilized.

Real-time Quantitative PCR (RT-qPCR) together with RNA Extraction

TRIzol reagent was used for the extraction of total RNA. Then cDNA was obtained from the RNA (10 ng in total) through reverse transcription using ReverTra Ace qPCR RT Kit, followed by enrichment of small RNAs via mirVana™ miRNA Isolation Kit to determine miR-148a. Next, SYBR Green PCR Premix was employed to perform RT-qPCR, and the ΔCT method was employed to measure miR-148a and HPIP for their expression levels, for which U6 small nuclear RNA plus GAPDH were set as the internal references, respectively. An ABI-7300 fluorescence quantitative PCR system was applied to conduct the reaction under the conditions below: 10 minutes of pre-denaturation at 95°C, together with 10 seconds at 95°C and 45 seconds at 60°C for 40 cycles.

Enzyme-linked Immunosorbent Assay (ELISA)

A 96-well plate was used to seed A549 cells (1×10^4/well in density). Upon reaching eighty percent confluence, the medium was replaced with serum-free medium. The supernatant was harvested after 48-hour incubation for ELISA (Penugurti et al. 2021).

Assay on Cell Proliferation

Cells were seeded at 2×10^3/well in density into a 96-well plate, of which the growth was determined using MTT assay kit daily within subsequent 5 days. Each well was added with MTT solution (5 mg/mL, about 10 μL) for 4 hours of cell incubation. Subsequently, 4-hour of cell incubation was conducted with each well added and fully mixed with 100 μL of formazan solution. Finally, a microplate reader was employed to detect the 570 nm wavelength to obtain the optical density (OD).

Cytotoxicity Assay

A 96-well plate was applied to inoculate normal and transfected A549 cells at 5×10^4/well in density until adherence. NK-92MI cells with proportions to lung cancer cells of 10:1, 5:1 and 2.5:1 were added. Subsequently, 10 μg/mL mouse ILT-2 antibody was added to block the binding of HPIP to ILT-2 of NK-92MI cells, while 1×PBS in an equal volume was added in the control group. After incubation for 4 hours, the density of living cells was determined by virtue of the MTT assay kit. Lysis rate=$[1-(OD_{E+T}-OD_E)/OD_T]\times100$ percent (Chen et al. 2022).

Transwell Assay

Cell suspension was prepared with the medium free of serum, which was loaded into the chamber of an 8-μm pore size Millicell Culture Plate Insert, with 3×10^4 cells in each chamber. The chamber was cultured for 24 hours with complete medium in a 24-well plate. The cells invading through the filter membrane into the lower chamber were fixed with formalin and subjected to 0.1 percent crystal violet staining. Subsequently, an optical microscope (400×) was employed to randomly select five visual fields to observe the cells and count the invading cells (Yun et al. 2020).

Colony Formation Assay

The complete medium containing 0.5 percent agar gel was added to a 24-well plate, and the medium containing 0.3 percent agar was used to prepare 5×10^4/mL cell suspension. Afterward, every well was supplemented with 500 μL of cell suspension, followed by incubation for 10 days. Cell colony was stained using MTT assay kit, and five visual fields were randomly selected from each well for observation under an optical microscope to count the colonies.

Detection with Western Blotting for HPIP Expression Level

Precooled protein lysate was mixed with the harvested cell precipitation prior to 30 minutes of incubation on ice as well as 4°C centrifugation at 10,000 rpm. Then the BCA protein assay kit was applied to quantify the proteins in the aspirated supernatant, and the concentration of total protein was adjusted to prepare samples. Next, the proteins subjected to 90 V of electrophoresis were translocated to a PVDF membrane. Following sealing under five percent skim milk, the membrane was treated with 1 hour of room-temperature incubation on a shaker. Later, the membrane supple-

mented with corresponding antibody solution (diluted at 1:500) was incubated for 30 minutes at room temperature on a shaker, followed by overnight culture at 4°C. The next day, the membrane underwent washing, blending with secondary antibody solution (diluted at 1:5,000) as well as 2-hour room-temperature incubation on a shaker. The rinsed membrane was added with ECL solution in a proper volume and then reacted for 5 minutes in dark. Finally, a quantitative imager was utilized for result observation.

Dual-luciferase Reporter Gene Assay

pGL3 luciferase reporter vector was inserted with HPIP binding sequence. As a 24-well plate was inoculated with A549 cells (density: 1×10^5/well), 100 ng of pGL3 reporter gene vector and pRL-TK *Renilla* luciferase plasmid (20 ng), in addition to 100 nM miR-148a-mimic and overexpressed control, were added to all wells for co-transfection and incubation overnight. The cells were lysed with reporter gene specific lysate. Finally, the luciferase activity was detected by means of the system for dual-luciferase reporter gene assay, using that of *Renilla* luciferase plasmid as the standard (Zhang et al. 2020).

Xenotransplantation *in vivo*

Twenty-four BALB/c nude mice (5 weeks old) at an equal gender ratio were purchased from Shanghai Experimental Animal Centre in China (Certificate of Quality No. SCXK (Shanghai) 2020-0011). The SPF experiment lab was selected for feeding of mice under such conditions as forty to seventy percent humidity and room temperature (25 ± 2)°C, where food and water were provided freely. Subsequent to 1 week of adaptive feeding, the experiment was carried out with operations in line with the ethical guidelines for the use of animal experiment.

The 24 nude mice were divided into A549+NK-92MI, A549+NK-92MI+ILT-2, A549 (si-HPIP)+NK-92MI and A549(si-HPIP)+NK-92MI+ILT-2 groups (n=6). Firstly, the nude mice in corresponding groups were subcutaneously inoculated with normal or transfected A549 cells at a density of 1×10^6/0.1 mL 1×PBS on the back. Then NK-92MI cells were seeded into all the mice from the caudal vein at a density of 1×10^7/0.1 mL 1×PBS 2 weeks later. In A549+NK-92MI+ILT-2 and A549 (si-HPIP)+NK-92MI+ILT-2 groups, 10 mg/kg ILT-2 antibody was administered through intraperitoneal injection, and the other two groups were injected with the same amount of 1×PBS at the same position, once a week. The following formula was adopted for the calculation of tumour volume conducted once weekly: volume=length×width^2×0.5. Four weeks following NK cell injection, the mice were anesthetised with isoflurane and then euthanised.

Statistical Analysis

The statistical analysis was accomplished by means of the SPSS 22.0 software. The mean ± standard deviation ($\chi \pm s$) was selected as the expression format for measurement data. The comparisons between two groups and among multiple groups were achieved via independent-samples *t*-test and one-way analysis of variance (ANOVA), respectively. The inter-group multivariate analysis was performed using repeated-measures ANOVA (Bonferroni corrected). The statistically significant differences were denoted with $P<0.05$.

RESULTS

Poor OS of NSCLC Patients with High HPIP Expression

The HPIP level changes in NSCLC patients were investigated through the simulation verification method of KMPlot database. The meta-analysis of cohort studies indicated the correlation between high HPIP expression and poor OS in NSCLC patients. HPIP had no correlation with OS of patients with squamous cell carcinoma. OS was significantly shortened in stage I and II NSCLC patients with high HPIP expression ($p<0.001$), but the influence of HPIP expression level on OS of patients with stage III NSCLC was not found. Besides, bioinformatics analysis was not carried out because of a small number of stage IV NSCLC patients as the samples (n=4, unavailable data). HPIP was able to forecast the survival of NSCLC patients, according to the large-scale data analysis results. Figure 1 presents the survival curves of NSCLC patients. All patient groups and different histopathological subgroups exhibited correlations between HPIP and overall survival probability.

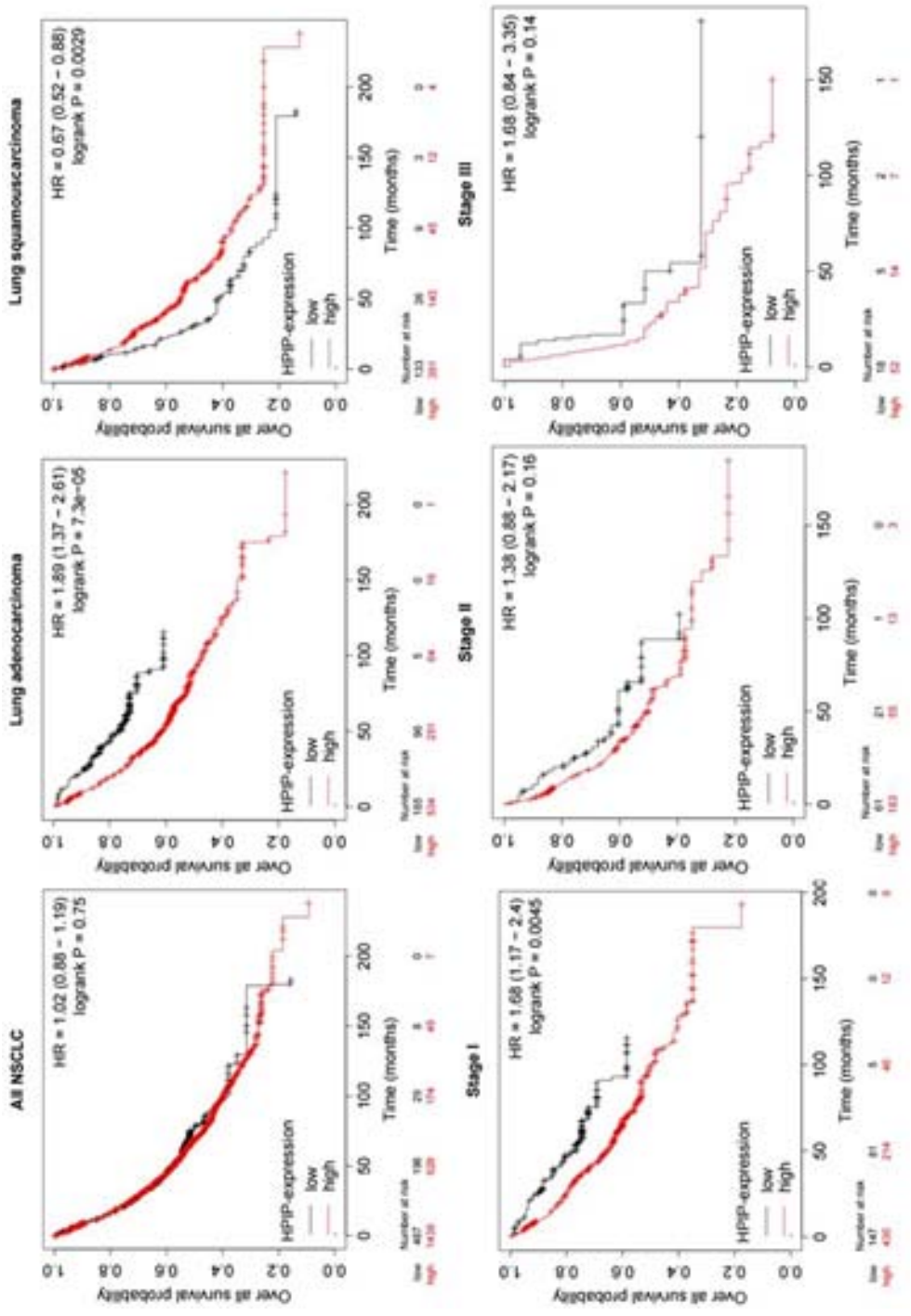

Fig. 1 . HPIP was a prognostic marker of NSCLC. Kaplan-Meier curves were generated using the KMPlot database. All patient groups and different histopathological subgroups exhibited correlations between HPIP and overall survival probability. HR: hazard ratio

HPIP Levels Related to miR-148a Expression plus Tolerance to Cytolysis Mediated by NK Cells

All three cell lines were subjected to HPIP and miR-148a detection. It was manifested in Figure 2A-C that the difference in miR-148a was not significant among A549, L78 and H460 cells at the relative expression level ($p>0.05$), but A549 cells had the lowest miR-148a expression whereas significantly higher expressions of HPIP mRNA, HPIP protein and sHPIP than those of L78 and H460 cells ($p<0.001$).

The resistance of NSCLC cells to NK-92MI cell lytic activity increased with reducing effector-to-target ratios ($p<0.05$). A549 cells had significantly higher resistance to NK-92MI cells than those of L78 and H460 cells at higher effector-to-target ratios ($p<0.05$). The three NSCLC cells exhibited similar tolerance to NK-92MI cells at a low effector-to-target ratio (2.5) (Fig. 2D). These findings suggested the correlations of HPIP expression with miR-148a level besides tolerance to cytolysis mediated by NK cells.

MiR-148a Inhibited NSCLC Cells in Terms of the Malignant Characteristics

Luciferase and Western blotting were employed to verify the regulatory effect of miR-148a on HPIP target genes. The luciferase activity of A549 cells carrying wild-type HPIP (HPIP-wt) was

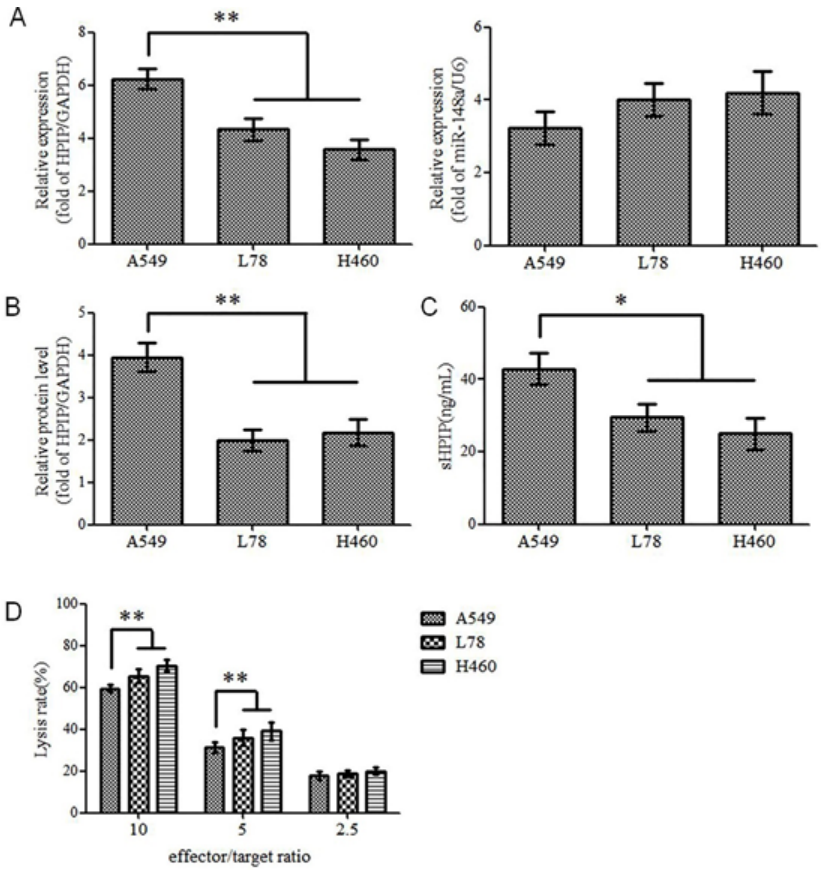

Fig. 2. HPIP was related to miR-148a level and tolerance to NK cell-mediated cytolysis. A) Relative expression levels of HPIP mRNA and miR-148a in different NSCLC cell lines. B) HPIP protein levels and C) sHPIP levels in the three cell lines. D) NK cell-mediated cytolysis for three cell lines. *$p<0.05$ and **$p<0.01$ *vs.* A549 group

inhibited, and HPIP presented a reduced relative expression level by contrast to those in control blank group ($p<0.05$). No impact was found in the luciferase activity of A549 cells carrying mutate HPIP (HPIP-mut), and there were no remarkable variations in the relative expression level of HPIP ($p>0.05$), indicating the ability of miR-148a to directly target HPIP. There was a negative regulatory effect of miR-148a on HPIP levels (Fig. 3). The abilities of proliferation, migration and colony formation were significantly weaker in A549 cells presenting overexpressed miR-148a but significantly higher in those with lowly expressed miR-148a, with comparison to those in the blank control group ($p<0.001$) (Figs. 4A-C). Moreover, the tolerance of A549 cells to NK cell-mediated cytolysis was affected by the abnormal miR-148a expression. The blank control group had a cell lysis rate of 60.21 percent when the effector-to-target ratio was 10, which increased to 74.38 percent in the group of miR-148a-mimics ($p<0.05$). Furthermore, the miR-148a-mimics group displayed a significantly raised cell lysis rate at an effector-to-target ratio of 5 ($p<0.05$), whereas the miR-148a-inhibitors group

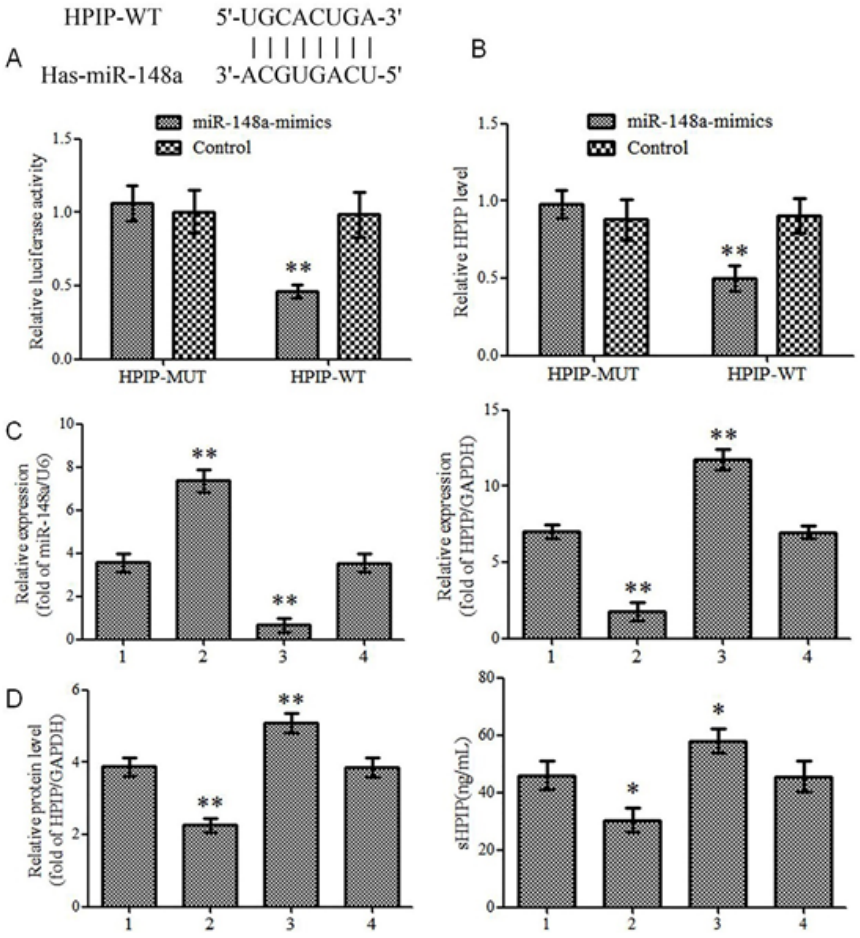

Fig. 3. MiR-148a regulated HPIP expression in A549 cells. A and B) Dual-luciferase reporter gene assay showed that HPIP was a direct target of miR-148a. C) Relative expression levels of miR-148a and HPIP in A549 cells with different transfections. D) HPIP protein levels and sHPIP levels in different transfected cells. 1: Blank; 2: MiR-148a-mimics; 3: MiR-148a-inhibitors; 4: Mock; $^{*}p<0.05$ and $^{**}p<0.01$ *vs.* HPIP-mut group and blank group

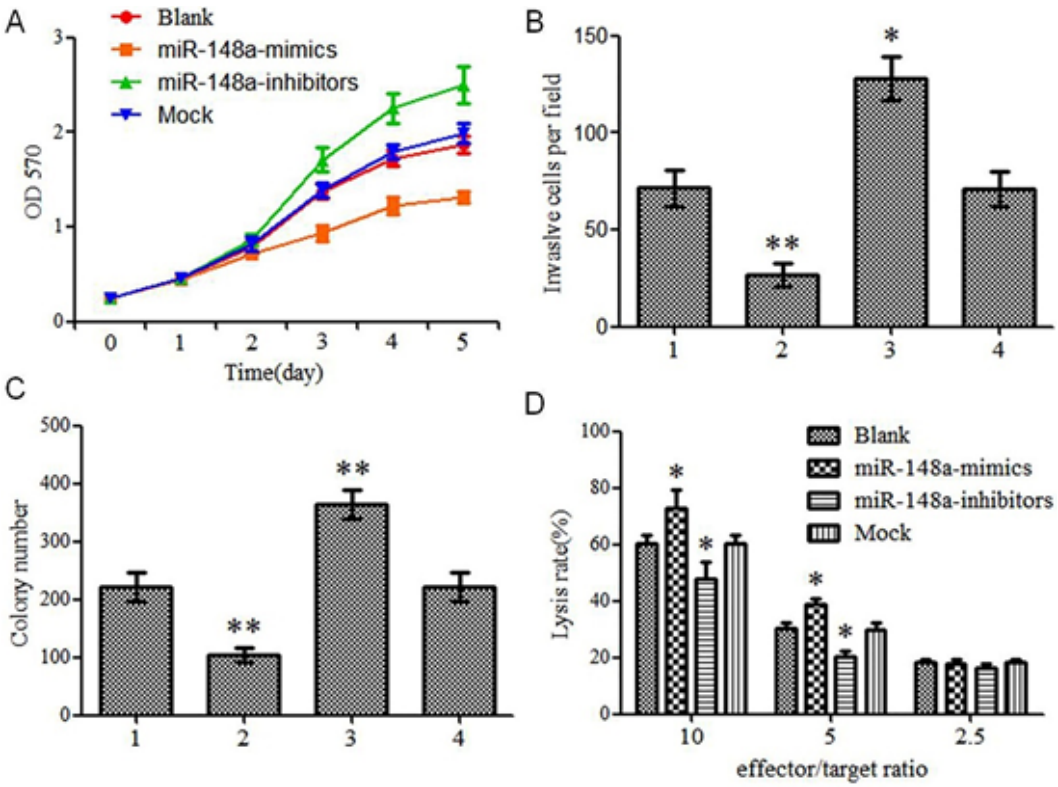

Fig. 4. MiR-148a inhibited the malignant characteristics of A549 cells. A) Effect of miR-148a on cell proliferation. B) Effect of miR-148a on cell migration (×400). C) Effect of miR-148a on colony formation. D) Effect of miR-148a on tolerance to NK cells. 1: Blank; 2: MiR-148a-mimics; 3: MiR-148a-inhibitors; 4: Mock; *p<0.05 and **p<0.01 *vs.* blank group

had an elevated cell lysis rate at higher effector-to-target ratios (p<0.05). Besides, the tolerance of A549 cells to NK cells was not influenced by miR-148a level (Fig. 4D). The above findings indicated that miR-148a could inhibit A549 cells from the aspect of malignant characteristics.

Effects on and Tolerance to NK Cells besides Cell Proliferation Exerted by HPIP-mediated miR-148a Inhibition

A549 cells were selected to knock down HPIP expression using siRNA technology to explore the timing of HPIP-mediated antitumor effect of miR-148a. HPIP level significantly decreased in si-HPIP group (p<0.001), but did not affect miR-148a expression (Fig. 5).

Interference with HPIP expression merely had impacts on the tolerance to NK cells (at effector-to-target ratios of 10 and 5, p<0.05) plus cell proliferation (p<0.05), but not cell migration or colony formation (Figs. 6A-C). The lysis rate of co-culture of lung cancer and NK cells was significantly higher than that in the blank control group added with PBS (all effector-to-target ratios, p<0.05). With the effector-to-target ratio set at 10, the cytotoxicity of NK cells in NK+si-HPIP and NK+anti-ILT-2 groups with inhibited HPIP expression and normal HPIP expression and addition of ILT-2 antibody increased significantly, but inhibiting HPIP expression or adding ILT-2 antibody did not further increase the lysis rate (Fig. 6D). The above findings demonstrate the influence of HPIP on colony formation/migration of cancer cells rather than their proliferation and immune escape.

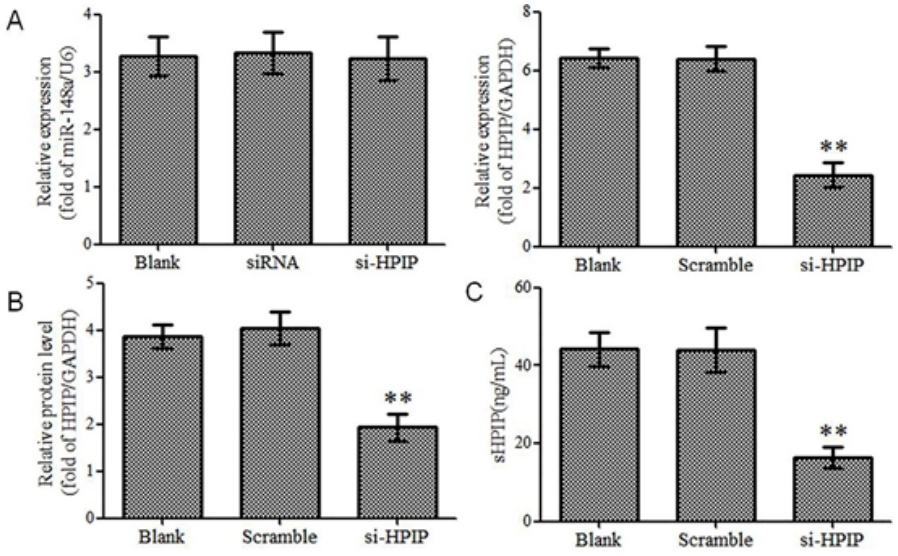

Fig. 5. Knockdown of HPIP expression in A549 cells. A) Relative expression levels of miR-148a and HPIP mRNA in different transfections. B) HPIP protein levels and C) sHPIP levels in different transfections $^{**}p<0.01$ *vs.* blank group

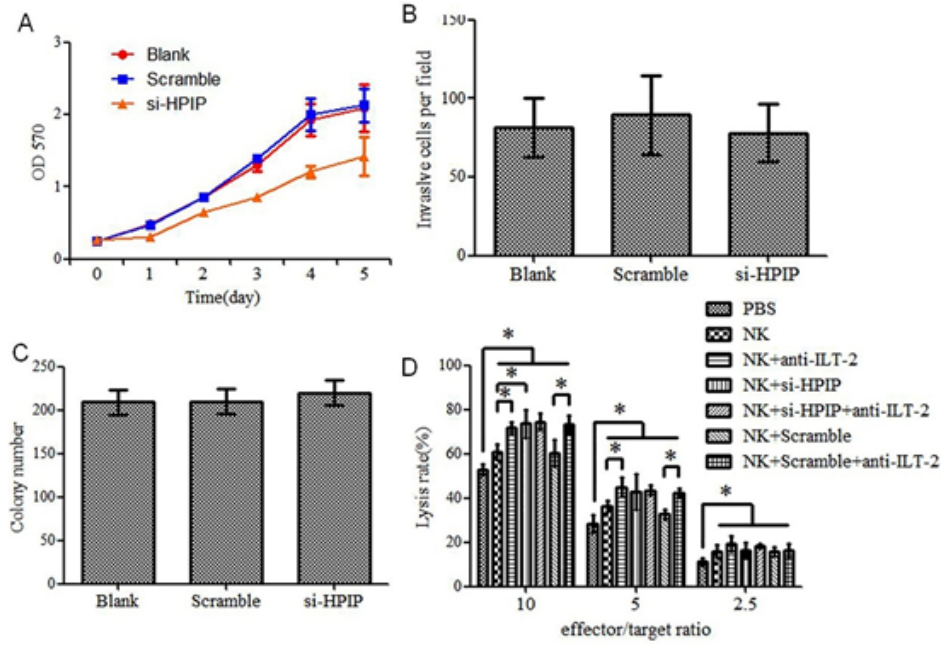

Fig. 6. HPIP affected cell proliferation and tolerance to NK cells under *in vitro* conditions. A) Effect of HPIP on cell proliferation. B) Effect of HPIP on cell migration (×400). C) Effect of HPIP on colony formation. D) Effect of HPIP on tolerance to NK cells. $^{*}p<0.05$ *vs.* PBS group

The mice from groups 1 and 2 receiving ordinary A549 cell inoculation presented significantly faster subcutaneous tumour growth than those from groups 3 and 4 inoculated with si-HPIP-transfected A549 cells, but no influence was found on the formation of subcutaneous tumours after injection of ILT-2 antibody. Meanwhile, the tumour growth of groups 1 and 2 was not notably different from that of groups 3 and 4. There was a relationship between HPIP expression and A549 cell proliferation as well as *in vivo* or *in vitro* immune escape. In the case of high HPIP expression, blocking the binding of HPIP to ILT-2 in NK cells can enhance their killing effect (Fig. 7).

DISCUSSION

It has been testified in NSCLC tissues that HPIP expression is in relation to not only disease stage but also survival time (Schulze et al. 2020). Besides, there is an association between disease stage and HPIP expression in NSCLC lesions, while sHPIP is related to survival time besides disease stage (Weissferdt et al. 2020). Moreover, HPIP level increases only in the case of NSCLC, especially squamous NSCLC (Tian et al. 2021). The findings mentioned above confirmed the correlations between HPIP and disease stage. Although immunohistochemistry and RT-qPCR can provide powerful evidence, the association between HPIP expression and histological type remains unclear, which is probably because a single study contains a small sample size. In this study, adenocarcinoma A549 cells exhibited an increased HPIP expression compared to L78 (squamous cell carcinoma cell) and H460 (large cell carcinoma cell), which supported the proposition that different histological types of NSCLC had different expressions of HPIP.

The correlations between HPIP expression and NK cells' killing effect have been confirmed in melanoma, choriocarcinoma, leuaemia, ovarian cancer and hepatocellular carcinoma (Konstantinopoulos et al. 2020; Rezaei et al. 2020; Short et al. 2020). The

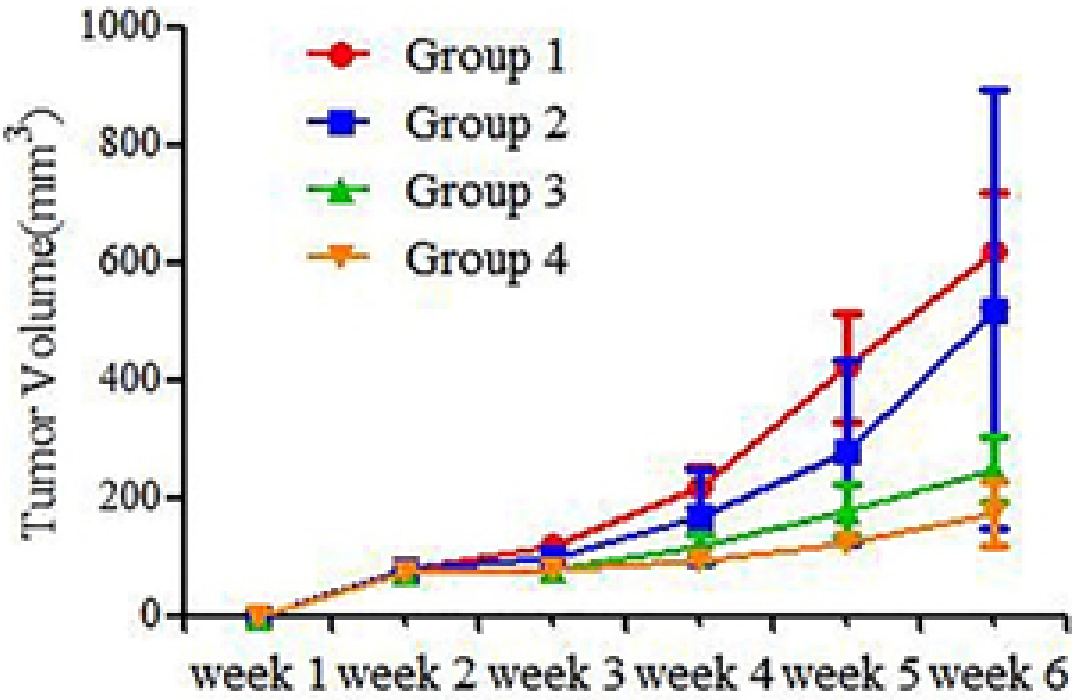

Fig. 7. HPIP affected cell proliferation and tolerance to NK cells under *in vivo* conditions

possibility of NK cells to lyse leukaemia cells depends on the expression level of HPIP. ILT-2/HPIP recognition is a crucial step for activating NK cells (Voutsadakis 2018). In this study, blocking the binding of ILT-2 to HPIP attenuated the lysis of A549 cells by NK cells *in vitro*. Despite NK cell proliferation depends on the stimulation signal of HPIP, silencing ILT-2 is capable of inhibiting NK cells from the aspect of *in vivo* and *in vitro* antitumor activity. Consistently, subcutaneous tumour size is primarily correlated with the HPIP expression level in tumour cells instead of ILT-2 inhibition. In addition to overexpression, low HPIP expression may be another mechanism by which tumour cells escape from NK cells' killing effect. It has been reported that HPIP is not expressed in most liver metastases of colorectal cancer, but overexpressed in primary tumour lesions (Fan et al. 2020; Lee et al. 2020).

Serum miR-148a is a well-documented biomarker for screening NSCLC and predicting the recurrence of resectable NSCLC (Joshi et al. 2015; Yang et al. 2015). Herein, HPIP regulated by miR-148a mediated the tolerance to NK cell-mediated cytolysis together with A549 cell multiplication, and miR-148a impacted the colony formation and movement of A549 cells as well. The correlations between these two aspects and HPIP remain uncertain. In the case of NSCLC, some miR-148a targets involving fibroblast growth factor-2 are down-regulated after miR-148a is overexpressed, and some NSCLC cell lines are suppressed in terms of movement and infiltration (Wang et al. 2020). Additionally, miR-148a can regulate the invasiveness of A549 cells by targeting neurofibromin-1, as well as target and regulate disintegrin and metalloproteinase-17 to suppress their migration, propagation, invasion and colony formation (Liu et al. 2020).

Regardless, there are several limitations in this study. Firstly, the regulating effects involving miR-148a plus HPIP were merely explored through cell experiment, and clinical samples were not tested. Therefore, the clinical values of HPIP and miR-148a should be further evaluated. Secondly, ILT-2 expression can also be detected from B cells and other immune cells on the surface. Hence, the ILT-2 expression in NK cells should be suppressed for future xenotransplantation studies.

CONCLUSION

In conclusion, HPIP is a prognostic marker of NSCLC. HPIP regulated by miR-148a can mediate the immune escape of A549 cells. In NSCLC, the miR-148a/HPIP axis influences cell propagation and mediates immune escape to play a carcinogenic role.

RECOMMENDATIONS

HPIP can be employed as a potentially eligible therapeutic target and immune checkpoint for NSCLC.

REFERENCES

Anft M, Netter P, Urlaub D et al. 2020. NK cell detachment from target cells is regulated by successful cytotoxicity and influences cytokine production. *Cell Mol Immunol,* 17(4): 347-355.

Chen T, Yang P, Chen HJ et al. 2022. A new biflavonoids from Aster tataricus induced non-apoptotic cell death in A549 cells. *Nat Prod Res*, 36(6): 1409-1415.

Duan W, Liu X 2020. PSAT1 upregulation contributes to cell growth and cisplatin resistance in cervical cancer cells via regulating PI3K/AKT signaling pathway. *Ann Clin Lab Sci*, 50(4): 512-518.

Elnaggar GN, El-Hifnawi NM, Ismail A et al. 2021. Micro RNA-148a targets Bcl-2 in patients with non-small cell lung cancer. *Asian Pac J Cancer Prev,* 22(6): 1949-1955.

Fan Z, Zheng W, Li H et al. 2020. LOXL2 upregulates hypoxia inducible factor 1α signaling through Snail FBP1 axis in hepatocellular carcinoma cells. *Oncol Rep,* 43(5): 1641-1649.

He W, Gong S, Wang X et al. 2021. DNA methylation integratedly modulates the expression of Pit-Oct-Unt transcription factors in esophageal squamous cell carcinoma. *J Cancer,* 12(6): 1634-1643.

Jiang K, Yang J, Yang C et al. 2020a. miR-148a suppresses inflammation in lipopolysaccharide-induced endometritis. *J Cell Mol Med,* 24(1): 405-417.

Jiang N, Dai Q, Su X et al. 2020b. Role of PI3K/AKT pathway in cancer: The framework of malignant behavior. *Mol Biol Rep*, 47(6): 4587-4629.

Joshi P, Jeon YJ, Laganà A et al. 2015. MicroRNA-148a reduces tumorigenesis and increases TRAIL-induced apoptosis in NSCLC. *Proc Natl Acad Sci USA,* 112(28): 8650-8655.

Kalani K, Yadav DK, Alam S et al. 2021. In-silico studies and Wet-Lab validation of camptothecin derivatives for anticancer activity against liver (HepG2) and lung (A549) cancer cell lines. *Curr Top Med Chem,* 21(10): 908-919.

Konstantinopoulos PA, Norquist B, Lacchetti C et al. 2020. Germline and somatic tumor testing in epithelial ovarian cancer: ASCO guideline. *J Clin Oncol,* 38(11): 1222-1245.

Lee HO, Hong Y, Etlioglu HE et al. 2020. Lineage-dependent gene expression programs influence the immune landscape of colorectal cancer. *Nat Genet,* 52(6): 594-603.

Li B, Feng F, Jia H et al. 2021. Rhamnetin decelerates the elimination and enhances the antitumor effect of the molecular-targeting agent sorafenib in hepatocellular car-

cinoma cells via the miR-148a/PXR axis. *Food Funct*, 12(6): 2404-2417.
Liu SD, Zhong LP, He J et al. 2020. Targeting neuropilin-1 interactions is a promising anti-tumor strategy. *Chin Med J (Engl)*, 134(5): 508-517.
Pan LN, Ma YF, Li Z et al. 2021. KRAS G12V mutation upregulates PD-L1 expression via TGF-β/EMT signaling pathway in human non-small-cell lung cancer. *Cell Biol Int*, 45(4): 795-803.
Penugurti V, Khumukcham SS, Padala C et al. 2021. HPIP protooncogene differentially regulates metabolic adaptation and cell fate in breast cancer cells under glucose stress via AMPK and RNF2 dependent pathways. *Cancer Lett*, 518: 243-255.
Phillips-Chavez C, Watson M, Coward J et al. 2020. A systematic literature review assessing if genetic biomarkers are predictors for platinum-based chemotherapy response in ovarian cancer patients. *Eur J Clin Pharmacol*, 76(8): 1059-1074.
Rezaei N, Neshasteh-Riz A, Mazaheri Z et al. 2020. The combination of metformin and disulfiram-cu for effective radiosensitization on glioblastoma cells. *Cell J*, 22(3): 263-272.
Roeper J, Falk M, Chalaris-Rißmann A et al. 2020. TP53 comutations in EGFR mutated patients in NSCLC stage IV: A strong predictive factor of ORR, PFS and OS in EGFR mt+ NSCLC. *Oncotarget*, 11(3): 250-264.
Schulze AB, Schmidt LH, Heitkötter B et al. 2020. Prognostic impact of CD34 and SMA in cancer-associated fibroblasts in stage I-III NSCLC. *Thorac Cancer*, 11(1): 120-129.
Short NJ, Konopleva M, Kadia TM et al. 2020. Advances in the treatment of acute myeloid leukemia: New drugs and new challenges. *Cancer Discov*, 10(4): 506-525.
Tian Y, Zhai X, Yan W et al. 2021. Clinical outcomes of immune checkpoint blockades and the underlying immune escape mechanisms in squamous and adenocarcinoma NSCLC. *Cancer Med*, 10(1): 3-14.
Voutsadakis IA 2018. Expression and function of immune ligand-receptor pairs in NK cells and cancer stem cells: Therapeutic implications. *Cell Oncol*, 41(2): 107-121.
Wang J, Yao Y, Wang K et al. 2020. MicroRNA-148a-3p alleviates high glucose-induced diabetic retinopathy by targeting TGFB2 and FGF2. *Acta Diabetol*, 57(12): 1435-1443.
Wang RP, Wang XH, Li ZM et al. 2020. Changes in serum inflammatory factors, adiponectin, intestinal flora and immunity in patients with non-small cell lung cancer. *Eur Rev Med Pharmacol Sci*, 24(20): 10566-10572.
Weissferdt A, Pataer A, Vaporciyan AA et al. 2020. Agreement on major pathological response in NSCLC patients receiving neoadjuvant chemotherapy. *Clin Lung Cancer*, 21(4): 341-348.
Yang JS, Li BJ, Lu HW et al. 2015. Serum miR-152, miR-148a, miR-148b, and miR-21 as novel biomarkers in non-small cell lung cancer screening. *Tumour Biol*, 36(4): 3035-3042.
Yun HH, Kim S, Kuh HJ et al. 2020. Downregulation of BIS sensitizes A549 cells for digoxin-mediated inhibition of invasion and migration by the STAT3-dependent pathway. *Biochem Biophys Res Commun*, 524(3): 643-648.
Zhang J, Mao F, Zhao G et al. 2020. Long non-coding RNA SNHG16 promotes lipopolysaccharides-induced acute pneumonia in A549 cells via targeting miR-370-3p/IGF2 axis. *Int Immunopharmacol*, 78: 106065.
Zhao YM, Yang G, You L et al. 2020. Effect of hematopoietic pre-B-cell leukemia transcription factor interacting protein knockdown on proliferation, cell cycle and apoptosis in pancreatic cancer cells. *Zhongguo Yi Xue Ke Xue Yuan Xue Bao*, 42(1): 7-15.
Zhu C, Zhuang W, Chen L et al. 2020. Frontiers of ctDNA, targeted therapies, and immunotherapy in non-small-cell lung cancer. *Transl Lung Cancer Res*, 9(1): 111-138.

Paper received for publication in October, 2021
Paper accepted for publication in October, 2023